World's first experimental observation of a Kondo cloud

Physicists have been trying to observe the Kondo cloud quantum phenomenon for many decades. An international research team including a scientist from City University of Hong Kong (CityU) has recently developed a novel device that successfully measures the length of the Kondo cloud and even allows for controlling it. The findings can be regarded as a milestone in condensed matter physics, and may provide insights for understanding multiple impurity systems such as high-temperature superconductors.

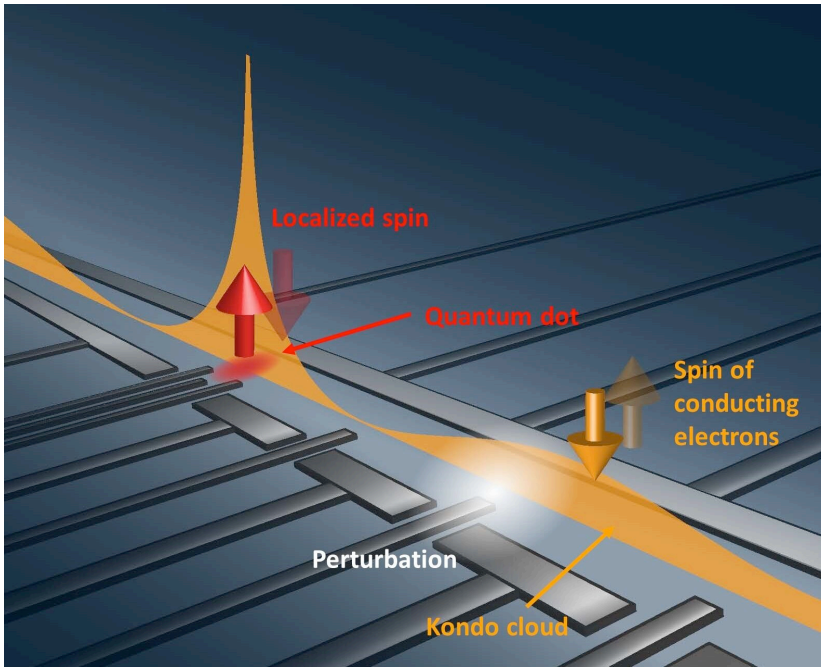

What is the Kondo cloud?

The Kondo effect is a physical phenomenon discovered in the 1930s. In metals, as the temperature drops, electrical resistance usually drops. However, if there are some magnetic impurities in the metal, it will show the opposite result. Resistance will drop at first. But when it is below some threshold temperature, the resistance will increase as the temperature decreases further.

This puzzle was solved over 50 years ago by Jun Kondo, a Japanese theoretical physicist for whom the effect was named. He explained that when a magnetic atom (an impurity) is placed inside a metal, it has a spin. But instead of just coupling with one electron to form a pair of spin-up and spin-down, it couples collectively with all the electrons within some areas around it, forming a cloud of electrons surrounding the impurity—this is called the Kondo cloud. When a voltage is applied over it, the electrons are not free to move or are screened off by the Kondo cloud, resulting in resistance increase.

How big is the cloud?

Some basic properties of the Kondo effect have been proven experimentally and were found to be related to the Kondo temperature (the threshold temperature where the resistance starts to go up at low temperature). However, the measurement of the Kondo cloud's length was yet to be achieved. Theoretically, the Kondo cloud can spread out over several micrometers from the impurity in semiconductors.

"The difficulty in detecting the Kondo cloud lies in the fact that measuring spin correlation in the Kondo effect requires the fast detection of tens of gigahertz. And you cannot freeze time to observe and measure each of the individual electrons".

Isolating a single Kondo cloud in the device

Thanks to the advance in nanotechnology, the research team fabricated a device that can confine an unpaired electron spin (magnetic impurity) in a quantum dot, like a small conducting island with a diameter of only a few hundreds nanometers. "Since the quantum dot is very small, you can know exactly where the impurity is," said Dr. Borzenets.

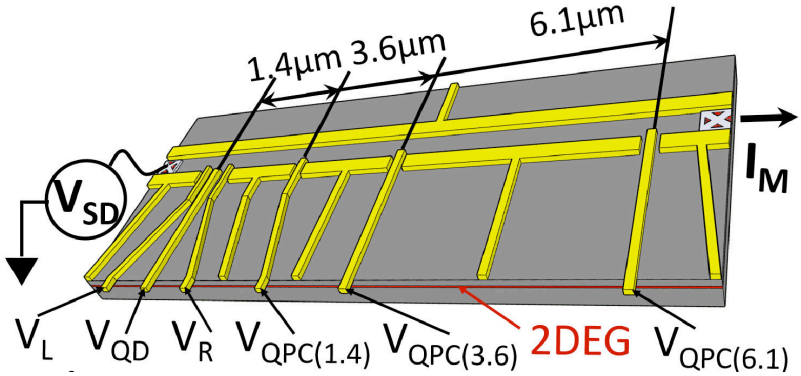

Connecting to the quantum dot is a one-dimensional and long channel. The unpaired electron is constricted to couple to the electrons in this channel and form a Kondo cloud there."In this way, we isolate a single Kondo cloud around a single impurity, and we can control the size of the cloud as well," he explained.

The novelty of the system is that by applying a voltage at different points inside the channel with various distances away from the quantum dot, they induced "weak barriers" along the channel. Researchers then observed the resulting change in electron flow and the Kondo effect with varying barrier strength and position.

The secret lies in the oscillation amplitude

By changing the voltages, it was found that the conductance went up and down, no matter where they put the barriers at. And when there were oscillations in conductance, oscillations in the measured Kondo temperature were observed.

When the researchers plotted the oscillation amplitude of Kondo temperature versus the barrier distance from the impurity divided by the theoretical cloud length, they found that all their data points fall onto a single curve, as theoretically expected. "We have experimentally confirmed the original theoretical result of the Kondo cloud length which is in micrometer scale," said Dr. Borzenets. "For the first time, we have proved the existence of the cloud by directly measuring the Kondo cloud length. And we found out the proportionality factor connecting the size of the Kondo cloud and Kondo temperature."

Provide insights into multiple impurity systems

The team spent almost three years in this research. Their next step is to investigate different ways to control the Kondo state. "Many other manipulations on the device can be done. For example, we can use two impurities at the same time, and see how they will react when the clouds overlap. We hope the findings can provide insights into the understanding of multiple impurity systems such as Kondo lattices, spin glasses and high transition-temperature superconductors."

Article

Observation of the Kondo screening cloud

https://doi.org/10.1038/s41586-020-2058-6

Received: 20 June 2019

Accepted: 11 December 2019

Published online: 11 March 2020

Check for updates

Ivan V. Borzenets[1,6]✉, Jeongmin Shim[2,6], Jason C. H. Chen[3], Arne Ludwig[4], Andreas D. Wieck[4], Seigo Tarucha[5], H.-S. Sim[2]✉ & Michihisa Yamamoto[5]✉

When a magnetic impurity exists in a metal, conduction electrons form a spin cloud that screens the impurity spin. This basic phenomenon is called the Kondo effect[1,2]. Unlike electric-charge screening, the spin-screening cloud[3–6] occurs quantum coherently, forming spin-singlet entanglement with the impurity. Although the spins interact locally around the impurity, the Kondo cloud can theoretically spread out over several micrometres. The cloud has not so far been detected, and so its physical existence—a fundamental aspect of the Kondo effect—remains controversial[7,8]. Here we present experimental evidence of a Kondo cloud extending over a length of micrometres, comparable to the theoretical length ξ_K. In our device, a Kondo impurity is formed in a quantum dot[2,9–11], coupling on one side to a quasi-one-dimensional channel[12] that houses a Fabry–Pérot interferometer of various gate-defined lengths L exceeding one micrometre. When we sweep a voltage on the interferometer end gate—separated by L from the quantum dot—to induce Fabry–Pérot oscillations in conductance we observe oscillations in the measured Kondo temperature T_K, which is a signature of the Kondo cloud at distance L. When L is less than ξ_K the T_K oscillation amplitude becomes larger as L becomes smaller, obeying a scaling function of a single parameter L/ξ_K, whereas when L is greater than ξ_K the oscillation is much weaker. Our results reveal that ξ_K is the only length parameter associated with the Kondo effect, and that the cloud lies mostly within a length of ξ_K. Our experimental method offers a way of detecting the spatial distribution of exotic non-Fermi liquids formed by multiple magnetic impurities or multiple screening channels[13–16] and of studying spin-correlated systems.

Although Kondo physics for a single magnetic impurity has been well established except for its spatial extension, our understanding of multiple impurity systems such as Kondo lattices, spin glasses, and high-transition-temperature (high-T_c) superconductors is far from complete. In such systems, the Kondo cloud length (or the spatial distribution of a Kondo cloud) with respect to the distance between impurities and other length parameters is crucial for an understanding of their properties. The detection and control of a Kondo cloud is therefore a milestone in condensed matter physics. There have been attempts to detect the Kondo cloud for 50 years[3–8,12,17–24]. Nuclear magnetic resonance measurements have not found any signature of the cloud[7]. Scanning tunnelling microscopy experiments have shown a signature of the Kondo effect but in a region a distance away from a magnetic impurity that is much shorter than the cloud length[17]. The difficulty lies in the fact that measuring spin correlation in the Kondo screening requires the fast detection of tens of gigahertz[18] and there may be complications arising from the atomic or electronic structures of the sample. However, recent advances in nanotechnology have opened up another way of detecting the Kondo cloud. We can now prepare a single spin in a quantum dot (QD) in contact with an electron reservoir, thus achieving systematic control of a single-channel Kondo state[9,10]. The theoretical value of the cloud length is typically[3] $\xi_K = \hbar v_F/(k_B T_K) \approx 1\,\mu m$ (where k_B is the Boltzmann constant) for $T_K \approx 1$ K and the Fermi velocity is $v_F \approx 10^5$ m s^{-1}. A recent theoretical study[25] of quantum entanglement shows that the Kondo state lies mostly within the distance ξ_K from the impurity, with a long algebraically decaying tail extending farther. Interesting proposals suggest the use of a finite-size electron reservoir, to observe competition between the cloud length and the reservoir size[19–21].

Here, instead of rigidly limiting the reservoir size, we perturb the reservoir by inducing a weak barrier at a position L far from the Kondo impurity and observe the resulting change in the Kondo effect with varying barrier position, following a recent proposal[12]. Figure 1a shows the device and measurement schemes. An unpaired electron spin (magnetic impurity) is confined in a QD coupled to a one-dimensional (1D), long, ballistic channel[26,27]. The QD is in the Coulomb blockade regime. The 1D channel is tuned to contain several conducting channels and has three quantum point contact (QPC) gates placed away from the QD at lengths $L = 1.4\,\mu m$, $3.6\,\mu m$ and $6.1\,\mu m$. Application of voltage V_{QPC} to one of the QPC gates creates a weak barrier so that a Fabry–Pérot (FP) cavity[28] of length L is formed between the QD and the QPC. The charging energy of the FP cavity is ineffective owing to strong coupling to the reservoir through multiple conducting channels. Changing V_{QPC} allows us to continuously tune the FP cavity between on- and off-resonances by altering the cavity length on the scale of the Fermi wavelength $\Delta L \approx \lambda_F$ (where

[1]Department of Physics, City University of Hong Kong, Kowloon, Hong Kong. [2]Department of Physics, Korea Advanced Institute of Science and Technology (KAIST), Daejeon, South Korea. [3]Department of Applied Physics, University of Tokyo, Tokyo, Japan. [4]Chair of Applied Solid State Physics, Faculty of Physics and Astronomy, Ruhr-University Bochum, Bochum, Germany. [5]Center for Emergent Matter Science (CEMS), RIKEN, Saitama, Japan. [6]These authors contributed equally: I. V. Borzenets, J. Shim. ✉e-mail: iborzene@cityu.edu.hk; hssim@kaist.ac.kr; michihisa.yamamoto@riken.jp

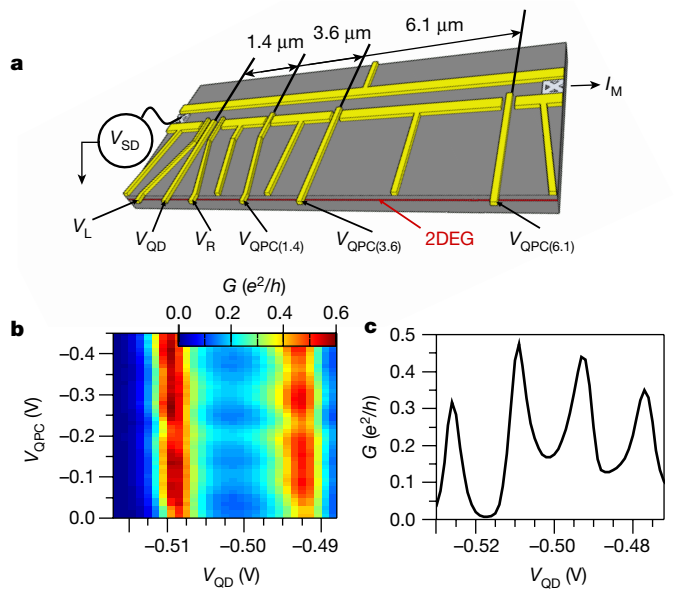

Fig. 1 | Measurement setup and characterization. a, Device and measurement schematic. The device consists of a QD coupled to a 1D channel (see Methods), in which three QPC gates are embedded at distances $L = 1.4$ μm, 3.6 μm and 6.1 μm from the QD. The activation of a QPC gate creates a FP cavity of length L. The QD is tuned via a central plunger gate voltage V_{QD} and two side gates V_L and V_R. The device is measured via the lock-in method: a small a.c. voltage V_{SD} is applied, and the current I_M through the system is measured. **b**, The conductance G (measured in units of quantum conductance, e^2/h) of the device versus the plunger gate voltage V_{QD} and the $L = 1.4$ μm QPC gate voltage V_{QPC}. Coulomb blockade peaks are observed with respect to changing V_{QD}. Oscillations associated with the FP cavity are seen with respect to changing V_{QPC}. **c**, Conductance G versus V_{QD} taken at $V_{QPC} = 0$. Coulomb blockade and a region of enhanced conductance around $V_{QD} = -0.50$ V associated with the Kondo valley are clearly observed.

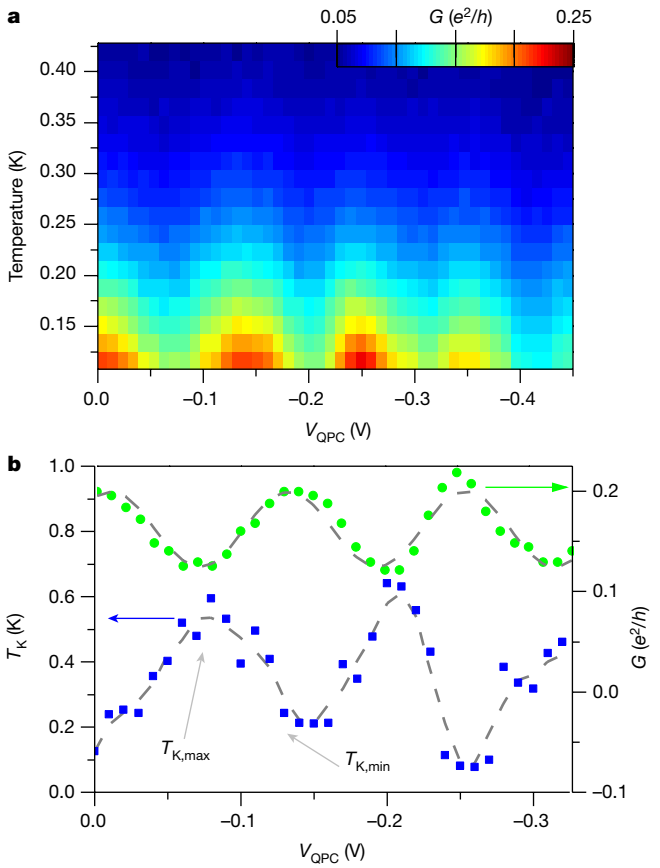

Fig. 2 | Influence of FP interference on the Kondo effect. a, Conductance G at the centre of the Kondo valley versus the QPC gate voltage V_{QPC} at $L = 1.4$ μm and device temperature T. G decreases with increasing T, indicative of the Kondo effect. For each V_{QPC}, the Kondo temperature T_K is extracted by fitting conductance versus temperature to an empirical formula[30]. **b**, Plot of the extracted T_K versus V_{QPC} (blue), shown alongside the conductance of the Kondo valley centre at base temperature G (green). T_K oscillates with respect to V_{QPC}, but in anti-phase with respect to conductance. The T_K oscillation amplitude is quantified by tracking the maximum $T_{K,max}$ and minimum $T_{K,min}$ of the first oscillation.

$\lambda_F \approx 40$ nm $<< L, \xi_K$) without affecting the potential profile around the QD. We find that changes in V_{QPC} strongly affect the measured Kondo temperature T_K when the cavity length L is shorter than $\xi_{K\infty} = \hbar v_F/(k_B T_{K\infty})$. Here $\xi_{K\infty}$ and $T_{K\infty}$ are the bare theoretical cloud length and bare Kondo temperature defined in the absence of the QPCs or equivalently for the case of $L = \infty$. For $L >> \xi_{K\infty}$, changes of V_{QPC} have little effect on T_K. This implies that the Kondo state extends over about $\xi_{K\infty}$.

The device is defined using top gates deposited on top of a GaAs/AlGaAs two-dimensional electron gas (2DEG) wafer, with an electron mean free path of about 8 μm (which is bigger than the device size). The QD population is controlled via a middle plunger gate voltage V_{QD}. The coupling of the QD to the 1D channel on the right side and to the left side is adjusted by changing the side gate voltages V_R and V_L, respectively. The QD is coupled more strongly to the right 1D channel than the left channel, so that the Kondo state is sensitive to the FP cavity of the 1D channel. We tune V_R to change the bare cloud length $\xi_{K\infty}$ and Kondo temperature $T_{K\infty}$. Figure 1c shows the conductance G between the right 1D channel and the left lead via the QD as a function of the plunger gate voltage V_{QD} when the QPCs are turned off. Several Coulomb blockade peaks are clearly visible with the measured charging energy of >500 μeV (ref. [29]). The Kondo effect is observed, manifesting itself in increased conductance in the valley region between two Coulomb blockade peaks[2,9,10]. The effect of the QPC gates is shown in Fig. 1b, which plots the conductance G versus plunger gate voltage V_{QD} as well as the voltage V_{QPC} applied to the QPC gate at $L = 1.4$ μm. Both the Coulomb blockade peaks as well as the Kondo valley undergo FP oscillations with respect to changing V_{QPC}; we note that at small V_{QPC} (equivalent to the first few FP oscillations) there is no effect on the QD energy level. The resonance level spacing $\Delta \approx 300$ μeV estimated from the data is consistent with the cavity length $L = 1.4$ μm, considering that $v_F = 2.46 \times 10^5$ m s^{-1}. The resonance level broadening of about 80 μeV implies a weak barrier formed by V_{QPC} (Supplementary Information).

To see the effect of the FP oscillations on the Kondo state, we measure the conductance G around the centre of the Kondo valley as a function of the QPC gate voltage V_{QPC} at different temperatures T (Fig. 2a). The valley conductance decreases with increasing temperature, indicative of the Kondo state. For each value of V_{QPC} we extract T_K around the valley centre by fitting conductance G versus temperature T to a well known empirical formula (see Methods)[30]. This method of extracting T_K is applicable for constant density of states of the reservoirs, but is still applicable to our QD coupled to the FP cavity, because the resonance level broadening is sufficiently large or the QPC barrier is weak (see Methods). We find that the Kondo temperature T_K undergoes oscillations with respect to changing V_{QPC} (Fig. 2b). Clearly, the Kondo state is affected by the perturbation at a location micrometres distant from the QD. The oscillation shows that the electron density of the FP cavity at the Fermi level that is coupled with the Kondo impurity differs between on and off resonances. This implies that the Kondo coherence is extended through the entire FP cavity, supporting the picture of the spatial extension of the Kondo cloud. It also implies that the resonance level spacing Δ is larger than the Kondo temperature, as theoretically expected. We note that, based on the scatter in T_K versus

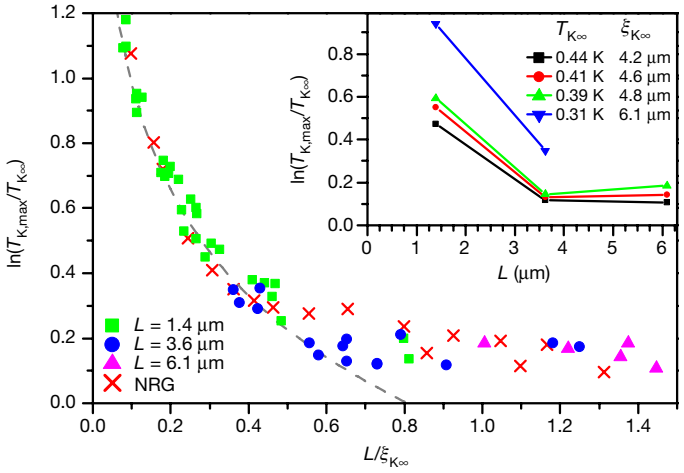

Fig. 3 | Shape of the Kondo cloud revealed from modulation of the Kondo temperature. Oscillation amplitude of T_K as a function of the FP cavity length L. The amplitude is quantified by $\ln(T_{K,max}/T_{K\infty})$, the maximum value $T_{K,max}$ of the oscillation normalized by the bare Kondo temperature $T_{K\infty}$ in logarithmic scale, and L is scaled by the bare Kondo cloud length $\xi_{K\infty}$. We note that $T_{K\infty}$ is estimated as $T_{K\infty} = (T_{K,max}T_{K,min})^{\frac{1}{2}}$ (see Supplementary Information). The green squares are obtained from the oscillation of T_K with respect to changes in the voltage V_{QPC} of the QPC gate located at $L = 1.4$ μm from the QD, the blue circles are for $L = 3.6$ μm, and the magenta triangles are for $L = 6.1$ μm. Different data points of the same symbol correspond to different $T_{K\infty}$ (that is, different settings of V_R and V_L). The data are compared with the theoretical results of the NRG calculation (red crosses) and the scaling of $\ln(T_{K,max}/T_{K\infty}) = -\eta\ln(L/\xi_{K\infty})$ with $\eta = 0.47$ (dashed curve). The inset shows the same data as the oscillation amplitude of T_K versus the length L not scaled by $T_{K\infty}$. The different curves represent those having the same $T_{K\infty}$.

V_{QPC} (where a smooth curve is expected), we estimate an error for the extracted T_K of about 20%.

The oscillations of T_K are anti-phase with those of the conductance. This agrees with scattering theories combined with the Fermi liquid and numerical renormalization group (NRG) methods when the QD is coupled more strongly to the FP cavity than to the left channel (Supplementary Information). In the on-resonance situations where the Fermi momentum k_F satisfies $e^{i2k_FL} = 1$, the FP cavity supports a maximum amount of electrons at the Fermi level, and hence the Kondo state with maximum Kondo temperature is developed. The development effectively changes the resonance condition to off-resonance, resulting in a minimum value of the conductance, since the electrons gain twice the scattering phase shift π/2 off the Kondo impurity in the QD[31]. The opposite happens in the off-resonance situations of $e^{i2k_FL} = -1$. We note that evidence of the Kondo scattering phase π/2 has been observed[26], and that the antiphase in Fig. 2b can be considered as further evidence. To quantify the effect of the FP cavity on the Kondo state we track the maximum $T_{K,max}$ and minimum $T_{K,min}$ of the first oscillation of T_K. Only the first oscillation is used because the subsequent oscillations require a higher V_{QPC}, which will have a stronger effect on the QD owing to capacitive coupling through the FP interferometer island.

We now discuss the dependence of the oscillation amplitude of T_K on the FP cavity length L shown in the inset of Fig. 3. The amplitude is quantified by $\ln(T_{K,Max}/T_{K\infty})$, and we estimate the bare Kondo temperature from the oscillation as $T_{K\infty} = (T_{K,max}T_{K,min})^{\frac{1}{2}}$ (see Supplementary Information for a validation of the estimate); $T_{K\infty}$ is not directly accessible because a QPC gate can form a barrier even when its voltage is turned off. The oscillation amplitude is small, that is, $T_{K,max} \simeq \approx 1.1T_{K\infty}$ or $T_{K,max} \simeq 1.2T_{K,min}$ for cavity lengths $L = 3.6$ μm and 6.1 μm and $T_{K\infty} = 0.39$–0.44 K. By contrast, the amplitude becomes much larger for $L = 1.4$ μm, for example, $T_{K,max} \simeq 3.2T_{K\infty}$ or $T_{K,max} \simeq 10T_{K,min}$ for $T_{K\infty} = 0.31$ K. For each L, the amplitude becomes larger as $T_{K\infty}$ is smaller. The result shows that the Kondo state is sensitive (oscillation amplitude of >30%) to the perturbation at distance $L \lesssim 3.6$ μm for $T_{K\infty} = 0.39$–0.44 K, while also sensitive at $L > 3.6$ μm for $T_{K\infty} = 0.31$ K. This implies that the cloud length is close to 3.6 μm for $T_{K\infty} = 0.39$–0.44 K, while larger than 3.6 μm for $T_{K\infty} = 0.31$ K. This finding is consistent with the bare cloud length $\xi_{K\infty}$ estimated by the theoretical relation of $\xi_{K\infty} = \hbar v_F/(k_B T_{K\infty})$, that is, $\xi_{K\infty} = 5.19$ μm, 4.12 μm, 3.92 μm and 3.65 μm for $T_{K\infty} = 0.31$ K, 0.39 K, 0.41 K and 0.44 K, respectively.

To see the universality of the results, we plot the oscillation amplitude of T_K versus the cavity length L scaled by the bare cloud length $\xi_{K\infty}$ in Fig. 3. Since we analyse only the first oscillation, the transmission through the QPC is almost independent of V_{QPC} and common for all QPCs. We find that all data points fall onto a single curve, as theoretically expected for a fixed transmission through the QPC. This scaling result is the evidence that ξ_K is the only length parameter associated with the Kondo effect. For $L \gtrsim \xi_{K\infty}$, the Kondo state is little affected by the perturbation at distance L, because the maximum of the oscillation is 20% larger than the minimum, $T_{K,max} \simeq 1.2T_{K,min}$. As L decreases below $\xi_{K\infty}$, the oscillation amplitude becomes very much larger, showing that the maximum is 1,000% larger than the minimum ($T_{K,max} \simeq 10T_{K,min}$) at $L \approx 0.1\xi_{K\infty}$ (we note that the oscillation amplitude is much bigger than the 20% error in the extracted T_K). The increase follows the universal scaling[12] of $\ln(T_{K,max}/T_{K\infty}) = -\eta\ln(L/\xi_{K\infty})$ with a constant η defined as the modulation of the density of states set by the QPC pinch-off strength. The plot is in good agreement with theoretical NRG calculations based on realistic parameters estimated from sample characterization (Supplementary Information). The result is consistent with the theoretical result[25] of the spatial distribution of the Kondo singlet entanglement that the main body of the Kondo cloud lies inside the length $\xi_{K\infty}$ with a long tail extending beyond $\xi_{K\infty}$. An equivalent, alternative picture is that for a FP cavity of length L, there are $L/\xi_{K\infty}$ (approximately $k_B T_{K\infty}/\Delta$) localized single-particle states of size $\xi_{K\infty}$ in a row. When $L/\xi_{K\infty} > 1$, the single-particle state located closest to the Kondo impurity forms the main body of the cloud and is wholly within L. Hence, the local perturbation at L affects only the other single-particle states contributing to the cloud tail. When $L/\xi_{K\infty} < 1$, the main body of the cloud extends beyond distance L and hence it is strongly affected by the perturbation.

Our result provides evidence of the spatial distribution of the Kondo state over micrometres. It will be interesting to study the spatial distribution further, for example, by engineering the spatial spin screening and the entanglement of the Kondo state. For example, by applying large QPC gate voltage to our device, we could systematically study the screening cloud of a Kondo box[19–21]. It will also be valuable to study the spin screening by multiple independent channels as in the multichannel Kondo effects or in a situation of multiple impurities as in the two-impurity Kondo effects, because those effects are accompanied by non-Fermi liquids and a quantum phase transition[13,14]. Our strategy of detecting spin screening by applying a weak electrostatic gate at a position distant from an impurity spin is applicable to the realization[15,16] of these effects with systematic control.

Our work is an initial measurement of a Kondo cloud. It may enable Kondo cloud detection in other systems and in other ways, such as by measuring spin–spin correlations. The universality implies that Kondo clouds in a conventional metal or in the mixed-valence regime have a spatial distribution similar to that found here, albeit with a shorter ξ_K. Ballistic electron transport over ξ_K will be required to apply our approach.

Online content

Any methods, additional references, Nature Research reporting summaries, source data, extended data, supplementary information, acknowledgements, peer review information; details of author contributions

and competing interests; and statements of data and code availability are available at https://doi.org/10.1038/s41586-020-2058-6.

1. Hewson, A. C. *The Kondo Problem to Heavy Fermions* (Cambridge Univ. Press, 1993).
2. Glazman, L. I. & Pustilnik, M. Low-temperature transport through a quantum dot. In *Nanophysics: Coherence and Transport* (ed. Bouchiat, H. et al.) 427–478 (Elsevier, 2005).
3. Affleck, I. The Kondo screening cloud: what it is and how to observe it. In *Perspectives of Mesoscopic Physics* (eds Aharony, A. & Entin-Wohlman, O.) Ch. 1, 1–44 (World Scientific Publishing, 2010).
4. Grüner, G. & Zawadowski, A. Magnetic impurities in non-magnetic metals. *Rep. Prog. Phys*. **37**, 1497–1583 (1974).
5. Gubernatis, J. E., Hirsch, J. E. & Scalapino, D. J. Spin and charge correlations around an Anderson magnetic impurity. *Phys. Rev. B* **35**, 8478 (1987).
6. Barzykin, V. & Affleck, I. The Kondo screening cloud: what can we learn from perturbation theory? *Phys. Rev. Lett*. **76**, 4959 (1996).
7. Boyce, J. P. & Slichter, C. P. Conduction-electron spin density around Fe impurities in Cu above and below T_K. *Phys. Rev. Lett*. **32**, 61 (1974).
8. Sørensen, E. S. & Affleck, I. Scaling theory of the Kondo screening cloud. *Phys. Rev. B* **53**, 9153 (1996).
9. Goldhaber-Gordon, D., Shtrikman, H., Mahalu, D., Abusch-Magder, D. & Meirav, U. Kondo effect in a single-electron transistor. *Nature* **391**, 156–159 (1998).
10. Cronenwett, S. M., Oosterkamp, T. H. & Kouwenhoven, L. P. A tunable Kondo effect in quantum dots. *Science* **281**, 540–544 (1998).
11. Kouwenhoven, L. P. & Glazman, L. I. Revival of the Kondo effect. *Phys. World* **14**, 33–38 (2001).
12. Park, J., Lee, S.-S. B., Oreg, Y. & Sim, H.-S. How to directly measure a Kondo cloud's length. *Phys. Rev. Lett*. **110**, 246603 (2013).
13. Cox, D. L. & Jarrell, M. The two-channel Kondo route to non-Fermi-liquid metals. *J. Phys. Condens. Matter* **8**, 9825–9853 (1996).
14. Affleck, I. Non-Fermi liquid behavior in Kondo models. *J. Phys. Soc. Jpn* **74**, 59–66 (2005).
15. Potok, R. M., Rau, I. G., Shtrikman, H., Oreg, Y. & Goldhaber-Gordon, D. Observation of the two-channel Kondo effect. *Nature* **446**, 167–171 (2007).
16. Iftikhar, Z. et al. Two-channel Kondo effect and renormalization flow with macroscopic quantum charge states. *Nature* **526**, 233–236 (2015).
17. Prüser, H. et al. Long-range Kondo signature of a single magnetic impurity. *Nat. Phys*. **7**, 203–206 (2011).
18. Borda, L. Kondo screening cloud in a one-dimensional wire: numerical renormalization group study. *Phys. Rev. B* **75**, 041307 (2007).
19. Thimm, W. B., Kroha, J. & von Delft, J. Kondo box: a magnetic impurity in an ultrasmall metallic grain. *Phys. Rev. Lett*. **82**, 2143 (1999).
20. Simon, P. & Affleck, I. Finite-size effects in conductance measurements on quantum dots. *Phys. Rev. Lett*. **89**, 206602 (2002).
21. Bomze, Yu. et al. Two-stage Kondo effect and Kondo-box level spectroscopy in a carbon nanotube. *Phys. Rev. B* **82**, 161411 (2010).
22. Holzner, A., McCulloch, I. P., Schollwöck, U., von Delft, J. & Heidrich-Meisner, F. Kondo screening cloud in the single-impurity Anderson model: a density matrix renormalization group study. *Phys. Rev. B* **80**, 205114 (2009).
23. Büsser, C. A. et al. Numerical analysis of the spatial range of the Kondo effect. *Phys. Rev. B* **81**, 045111 (2010).
24. Mitchell, A. K., Becker, M. & Bulla, R. Real-space renormalization group flow in quantum impurity systems: local moment formation and the Kondo screening cloud. *Phys. Rev. B* **84**, 115120 (2011).
25. Lee, S.-S. B., Park, J. & Sim, H.-S. Macroscopic quantum entanglement of a Kondo cloud at finite temperature. *Phys. Rev. Lett*. **114**, 057203 (2015).
26. Takada, S. et al. Transmission phase in the Kondo regime revealed in a two-path interferometer. *Phys. Rev. Lett*. **113**, 126601 (2014).
27. van der Wiel, W. G. et al. The Kondo effect in the unitary limit. *Science* **289**, 2105–2108 (2000).
28. van Houten, H. et al. Coherent electron focusing with quantum point contacts in a two-dimensional electron gas. *Phys. Rev. B* **39**, 8556 (1989).
29. Kouwenhoven, L. P. et al. Electron transport in quantum dots. In *Mesoscopic Electron Transport* (eds Sohn, L. L., Kouwenhoven, L. P. & Schön, G.) NATO Advanced Study Institutes Series E, Vol. 345, 105–214 (Kluwer Academic, 1997).
30. Goldhaber-Gordon, D. et al. From the Kondo regime to the mixed-valence regime in a single-electron transistor. *Phys. Rev. Lett*. **81**, 5225 (1998).
31. Noziéres, P. A Fermi-liquid description of the Kondo problem at low temperatures. *J. Low Temp. Phys*. **17**, 31–42 (1974).

Methods

Sample preparation

The system of the QD coupled to the quasi-1D FP resonant cavity was fabricated in a 2DEG (carrier density $n = 3.12 \times 10^{11}$ cm^{-2}, mobility $\mu = 0.86 \times 10^6$ cm^2 V^{-1} s^{-1}) heterointerface using a standard surface Schottky gate technique.

Measurement

Measurements were performed in an Oxford Instruments MX100 dilution refrigerator with a base lattice temperature of 40 mK. The base electron temperature was measured to be around 80 mK. (Electron temperature versus measured mixing chamber temperature was calibrated via analysis of the QD Coulomb blockade peak width.) The quasi-1D channels were formed by applying an approximately −0.45 V (−1 V) signal to the gates defining the bottom (top) boundary of the channel. (This voltage was sufficient to fully deplete the carriers below the gates, isolating the channel from the rest of the 2DEG.) Electron transport was measured using the lock-in method. An a.c. voltage oscillation with a d.c. offset was applied to a sample via a divider with the a.c. excitation set to 3–15 μV. The d.c. offset was set so as to achieve zero bias at the sample. (The d.c. offset was varied in order to calculate the QD charging energy.) Current through the sample was measured using a custom current sense amplifier with a current-sense resistor of 10 kΩ mounted on the mixing chamber. Gate voltages were controlled via a custom digital-to-analog converter (DAC). Temperature of the device was changed globally via a heating coil at the mixing chamber.

We provide additional details about the gate voltage settings (see Fig. 1a). The voltage applied to the long global gate defining the upper boundary of the 1D channels and the QD was fixed to about −1.0 V for the entire experiment. The gate voltages defining the left and right 1D channels from the lower side were set to about −0.45 V, fully depleting the carriers underneath the gates but leaving several conducting channels in each 1D wire. The gate voltages defining the QD were operated around −0.5 V, being varied in order to achieve different values of $T_{K\infty}$. The voltages on the tunnel coupling gates $V_{L,R}$ were set in a range of −0.45 V to −0.6 V, while the middle plunger gate voltage V_{QD} was swept between −0.4 V and −0.7 V. The QPC gates were set to zero voltage when not operated. We confirmed that $V_{QPC(1.4)}$ and $V_{QPC(3.6)}$ have no influence on the conductance through longer FP cavities defined by $V_{QPC(3.6)}$ or $V_{QPC(6.1)}$.

Calibration of measured sample temperature

For temperatures below about 500 mK it becomes increasingly difficult to thermalize hot electrons sent to the sample from the measurement electronics. In this measurement setup, the hot electrons were cooled at the mixing chamber via a thermalization coil as well as via copper powder filters. Nevertheless, calibration was required to match the measured mixing chamber lattice temperature to the actual electron temperature in the sample. This was achieved by measuring the shape of the Coulomb blockade peaks of the QD with all the QPCs turned off (Extended Data Fig. 1c). Picking a peak that does not feature any Kondo temperature, we should expect that the conductance $G(\delta V_G)$ (where δV_G is the shift in plunger gate voltage away from the Coulomb blockade peak centre) will be proportional to $\cosh^{-2}\left(\frac{(a\delta V_G)}{2k_BT}\right)$ (ref. [29]). The constant a is independent of electron temperature and should depend only on the sample geometry. (Extended Data Fig. 1a shows the fit of G versus gate voltage V_G taken at a measured temperature of $T_{measured} = 300$ mK). Indeed, above $T_{measured} > 600$ mK we see that a has little to no variation, so the mixing chamber thermometer temperature and the electron temperature are the same $T_{calibrated} = T_{measured}$. By looking at how the constant a evolves for $T_{measured} < 600$ mK we can now build the calibration for the electron temperature $T_{calibrated} = F(T_{measured})$ as shown in Extended Data Fig. 1b. Throughout the text, the temperature T refers to the calibrated temperature $T_{calibrated}$.

QPC barrier strengths

The strengths of the oscillations in $T_{K,max}/T_{K\infty}$ depends on the QPC pinchoff strength α. Here we define $\alpha = 1 - (t_0/t)^2$ with t_0 being the hopping energy across the QPC and t being the hopping energy along the 1D channel. ($\alpha = 0$ means there is no pinchoff present due to the QPC, and $\alpha = 1$ means that the QPC fully decouples the FP cavity from the rest of the wire. See the Hamiltonian in the Supplementary Information.) Below we estimate α in three different ways, which show $\alpha \approx 0.1$. Fitting the main results (Fig. 3) to the NRG calculations, we arrive at $\alpha \approx 0.1$. In addition, we find that α can be obtained from the ratio of on- and off-resonance conductances of the Kondo valley at $T = 0$ as follows: $\alpha = 1 - (G_{0,Min}/G_{0,Max})^{0.5}$. The conductances at zero temperature can be extracted similarly to T_K by fitting to the empirical formula[30] (see below for fitting details). Averaging the data over several values of V_L and V_R we arrive at $\alpha \approx 0.1$. Finally, we estimate α also by considering the behaviour of the system away from the Kondo regime. The strength is proportional to the fluctuations in the local carrier density ρ inside the FP cavity: $\alpha = 1 - (\rho_{min}/\rho_{max})^{0.5}$, where $\rho_{max(min)}$ is the maximum (minimum) value of the fluctuations in ρ. In turn, the effective coupling strength Γ_r of the QD to the FP cavity is proportional to the local carrier density ρ. The coupling strength Γ_r directly affects the width of the Coulomb blockade peak with respect to gate voltage V_G. Indeed, as we tune the FP resonance by changing the QPC gate voltage V_{QPC}, the Coulomb blockade peak undergoes fluctuations in width in synchrony with fluctuations in conductance (Extended Data Fig. 2). Taking the first oscillation, we arrive at the QPC pinchoff strength $\alpha = 1 - (W_{min}/W_{max})^{0.5} \approx 0.1$, where W is the width of the oscillation.

For the case of ballistic electron transport and a similar α for all three QPC gates, one would expect the amplitude of the FP oscillations in Coulomb-blockade peak conductance to be independent of the QPC gates at different distances. Indeed, when comparing the oscillations for the same settings of V_L and V_R, but activating QPC gates at the three different distances, we see that the amplitudes are within 15% of each other (Extended Data Table 1).

Kondo temperature estimation

The Kondo temperature T_K is estimated by fitting the experimental data to the empirical formula[30] of

$$G(T) = G_0\left(\frac{T_K'^2}{T^2 + T_K'^2}\right)^s$$

with $T_K' = T_K/\sqrt{2^{1/s} - 1}$, where the zero-temperature conductance G_0 and the exponent s are fitting parameters; according to ref. [30], the exponent s should not vary much from 0.22; in this sense, the fitting has only two fitting parameters, T_K and G_0. This estimation works well when the density of states of the reservoirs coupled to a Kondo impurity is approximately energy-independent near the Fermi level. In our setup, in which the Kondo impurity in the QD is coupled to the FP cavity, the density of states is energy-dependent and the estimation is applicable when the QPC barrier defining the FP cavity is so weak that the energy dependence is not crucial. The applicability of the estimation is confirmed by our NRG calculation with the model parameters chosen from the experimental data (Supplementary Information).

An example of the fit of our data to the empirical formula is shown in Extended Data Fig. 3, with T_K and G_0 as fitting parameters (Extended Data Table 2). (On average, the fitting function returned a degrees-of-freedom adjusted R^2 value of 0.995 for all the values of V_{QPC} within the first oscillation cycle.) The trend of G versus T is described well by the empirical formula with $s = 0.22 \pm 0.01$ (Extended Data Table 2).The fit is done with the temperature dependence of the conductance G over an electron temperature window of 0.1–0.5 K. In usual cases (namely, in the absence of the FP cavity), the conductance G measured within the temperature window $[0.5T_K, 1.5T_K]$ around the T_K is sufficient to

correctly estimate the Kondo temperature from the fit; this can be confirmed by using NRG calculations or by analysing the empirical formula. It is because this window can capture the Kondo crossover (from the Kondo fixed point to the local moment fixed point). Even with the FP cavity, this estimation is expected to work well in the regime of $L < 0.4\xi_{K\infty}$ according to our NRG calculation (Supplementary Information). The estimation becomes worse as L increases ($>0.4\xi_{K\infty}$), but not enough to affect our conclusion in the main text and Fig. 3.

We remark two points. First, while the fitting function implies a good fit, it is difficult to estimate the error in the fitted T_K from a single fit. Instead, as discussed in the main text, we obtain an error by looking at the scatter of T_K when the QPC voltage is changed. In an ideal case, the Kondo temperature is expected to evolve smoothly with QPC voltage. That is, for a small change in voltage ΔV_{QPC} we expect only a small deviation in temperature $T_K(V_{QPC}) \approx T_K(V_{QPC} + \Delta V_{QPC})$. Large changes in T_K for small changes in V_{QPC} are therefore attributed to error. Using this method, we arrive at an error in T_K of about 20%.

Second, the fitting parameter $s = 0.22$ implies that our experiment is in the Kondo regime rather than in the mixed-valence regime. The empirical formula provides a good fit with its parameter $s = 0.22$ in the Kondo regime, while the parameter deviates rapidly from 0.22 in the mixed-valence regime[30].

We note that the estimation of T_K directly from the experimental data is a merit of our experimental regime; it is unclear how to estimate T_K directly in the opposite regime where the QPC barrier is strong (corresponding to a finite-size reservoir coupled to a QD[19–21]). This is because the temperature dependence of the conductance G has a nontrivial feature due to the FP resonance when the QPC barrier is strong (the nontrivial feature is enhanced as the barrier becomes stronger, and the feature is not captured by the empirical formula), as shown in our NRG calculations.

Modelling

To model our experiments, we theoretically study an Anderson impurity formed in a QD coupled to two 1D leads, one of which houses a FP cavity. The Hamiltonian of the model is found in the Supplementary Information. The parameters of the model are estimated from the experimental data. The QD spectral function is obtained by using the NRG method, and the temperature dependence of the conductance is computed[1] by combining the spectral function and the Fermi–Dirac distribution function. The feature in Fig. 2 (that the oscillations of T_K are anti-phase with those of the conductance) is reproduced in our theory in two different ways. The feature is obtained by using the scattering-matrix formalism combined with the Fermi liquid theory and by taking into account the scattering phase shift π/2 off the Kondo impurity. The anti-phase feature is also found in an independent way based on the NRG method and conductance calculation. On the other hand, the NRG result of the Kondo temperature T_K in Fig. 3 is obtained, in the same way as for the experimental estimation of T_K, by fitting the conductance obtained by the NRG method to the empirical formula. The universal scaling behaviour in Fig. 3 is obtained by using the Poor Man's Scaling[12] and it is confirmed by NRG calculations; the Poor Man's Scaling and the NRG give the same scaling form but with different values of the parameter η, as η depends on the estimation method of T_K. The details are found in the Supplementary Information.

Universal scaling at $L < \xi_{K\infty}$

The experimental data in Fig. 3 show the behaviour of

$$\ln(T_{K,max}/T_{K\infty}) \approx -\eta \ln(L/\xi_{K\infty}) \quad (1)$$

at $L < \xi_{K\infty}$. This behaviour is scaled only by $T_{K\infty}$ and $\xi_{K\infty}$, so it is a universal feature characterizing the core region ($\hbar v_F/U < L < \xi_{K\infty}$) of the Kondo cloud. Here U is the QD charging energy (see Supplementary Information).

We derive the behaviour. In our experimental regime of $t_l << t_r$ and small α, the Poor Man's Scaling[12] leads to $\ln(T_{K,max}/T_{K\infty}) \approx -\alpha \ln(L/\xi_{K\infty})$. Here t_l (t_r) is the tunnelling amplitude between the QD and the left channel (the FP cavity). See Supplementary Information. In this estimation based on the Poor Man's Scaling, η equals α. This implies that the coefficient η is determined mainly by the resonance broadening parameter α for small α. The NRG calculation confirms the universal scaling in equation. (1), but with $\eta \neq \alpha$. The value of η depends on the estimation method of the Kondo temperature; the Kondo temperature is defined in the Poor Man's Scaling in a way that is different from that in the NRG method. We find that the scaling behaviour also occurs in the other regime of $t_{l,r}$ and α including the regimes of large α. We also note that at $L > \xi_{K\infty}$, the Kondo cloud has a long tail following another algebraic scaling law characterized by quantum entanglement or electron conductance[25,32].

Data availability

The data that support the findings of this study are available from the corresponding authors upon reasonable request.

32. Yoo, G., Lee, S.-S. B. & Sim, H.-S. Detecting Kondo entanglement by electron conductance. *Phys. Rev. Lett.* **120**, 146801 (2018).

Acknowledgements I.V.B. acknowledges CityU New Research Initiatives/Infrastructure Support from Central (APRC) (grant number 9610395), and the Hong Kong Research Grants Council (ECS) Project (grant number 21301818). S.T. and M.Y. acknowledge KAKENHI (grant number 38000131). M.Y. acknowledges KAKENHI (grant number 18H04284) and CREST-JST (grant number JPMJCR1876). S.T. acknowledges CREST-JST (grant number JPMJCR1675). M.Y. acknowledges discussions with R. Sakano. H.-S.S. acknowledges support by Korea NRF via the SRC Center for Quantum Coherence in Condensed Matter (grant number 2016R1A5A1008184). A.L. and A.D.W. acknowledge support from DFG-TRR160,BMBF—Q.Link.X16KIS0867 and DFH/UFA CDFA-05-06.

Author contributions I.V.B. performed the experimental measurements and analysed experimental data. J.S. and H.-S. S. performed the theoretical calculations. J.C.H.C. fabricated and characterized the device. A.L. and A.D.W. designed and grew the 2DEG wafer. M.Y. designed the experiment. M.Y. and S.T. supervised the project. All authors were involved in discussing results and preparing the manuscript.

Competing interests The authors declare no competing interests.

Additional information
Supplementary information is available for this paper at https://doi.org/10.1038/s41586-020-2058-6.
Correspondence and requests for materials should be addressed to I.V.B., H.-S.S. or M.Y.
Peer review information *Nature* thanks GuoPing Guo, Robert Peters and the other, anonymous, reviewer(s) for their contribution to the peer review of this work.
Reprints and permissions information is available at http://www.nature.com/reprints.

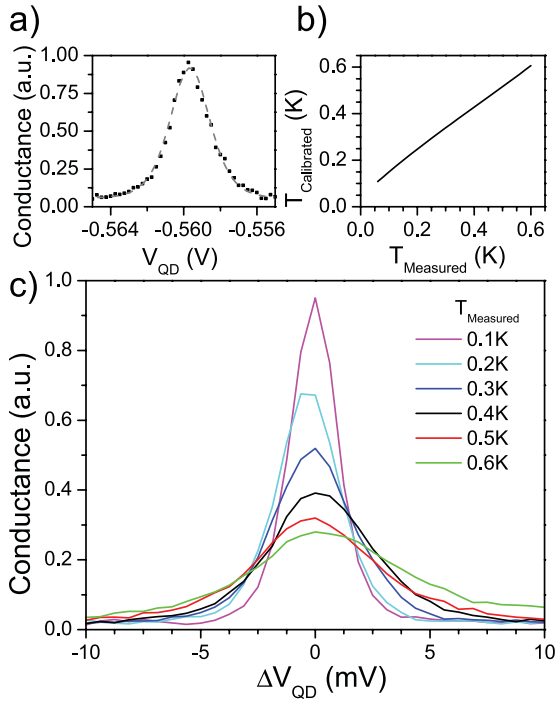

Extended Data Fig. 1 | Calibration of measured sample temperature. **a**, Conductance versus QD gate voltage V_G taken at a temperature of 300 mK. The grey lines show the fit of the data to the theoretical lineshape for a Coulomb blockade peak. **b**, The electron temperature in our device $T_{calibrated}$ versus the lattice temperature measured by a thermometer located at the mixing chamber $T_{measured}$. **c**, Conductance of the Coulomb blockade peaks versus gate voltage (around the peak centre) δV_G shown for several values of the measured temperature. (a.u., arbitrary units).

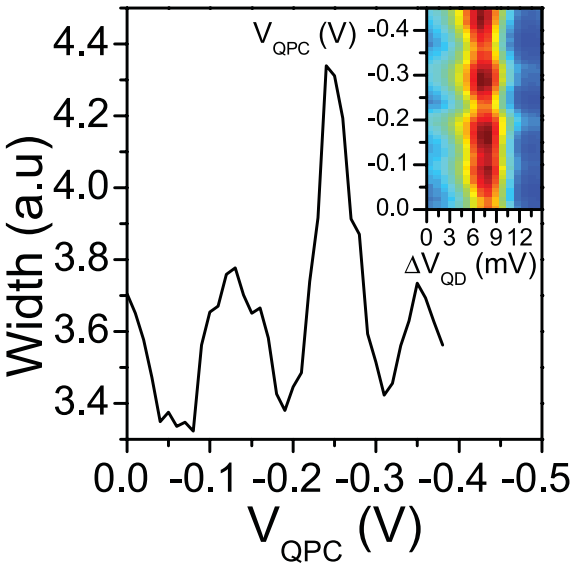

Extended Data Fig. 2 | Full width at half maximum of a Coulomb blockade peak versus QPC gate voltage V_{QPC}. Data are shown for a Coulomb blockade peak away from the Kondo valley. The inset shows conductance G through the QD as a function of (shifted) gate voltage δV_G and QPC gate voltage V_{QPC}. Oscillations of both peak conductance and peak width with respect to V_{QPC} are clearly observed.

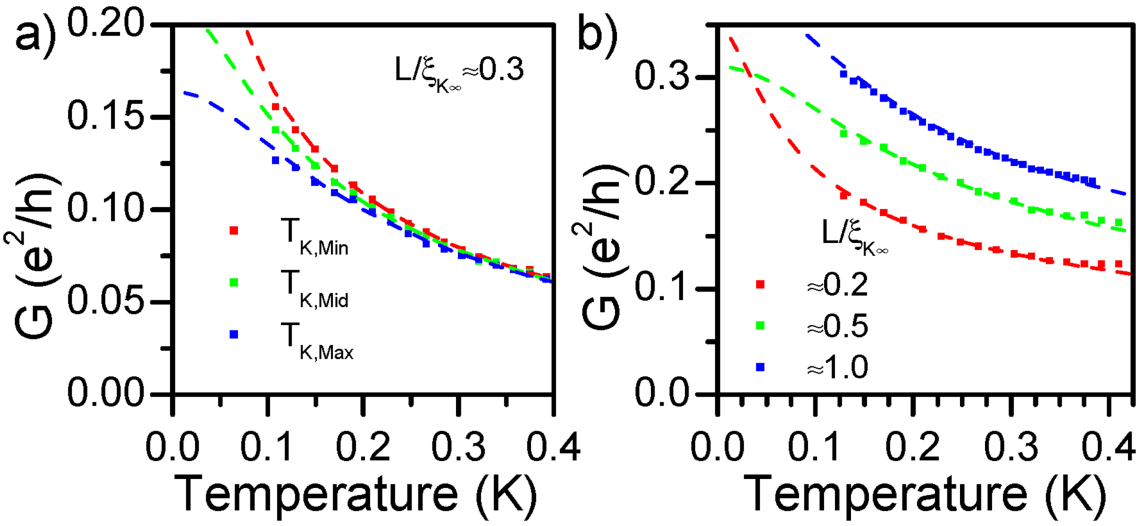

Extended Data Fig. 3 | Plot of conductance versus temperature at the centre of the Kondo valley. The lines are fits to the empirical formula. **a**, The data in red correspond to V_{QPC}, at which the minimum Kondo temperature was observed. The data in blue correspond to V_{QPC}, at which the maximum Kondo temperature was observed. Green data points correspond to data taken at a midpoint beween the red and blue datasets. **b**, Data at $V_{QPC} = 0$ V, for several QD settings corresponding to different $L/\xi_{K\infty}$.

Extended Data Table 1 | Coulomb-blockade peak FP oscillation amplitude

QPC distance L	Oscillation amplitude ΔG
1.4 μm	0.080 e^2/h
3.6 μm	0.073 e^2/h
6.1 μm	0.071 e^2/h

The amplitude of FP oscillations in Coulomb-blockade peak conductance versus distance to the QPC gates.

Extended Data Table 2 | Fitting parameters with upper and lower bounds

Fitting Parameter	Lower Bound	Upper Bound
Kondo Temperature T_K	0K	1.2K
Conductance at $T = 0$ G_0	0	e^2/h
Power Law Factor s	0.21	0.23